

# The Role of Crosslinker Molecular Structure on Mechanical and Light-Actuation Properties in Liquid Crystalline Networks

Simone Donato, Daniele Martella,\* Martina Salzano de Luna, Giulia Arecchi, Silvia Querceto, Cecilia Ferrantini, Leonardo Sacconi, Pierre-Louis Brient, Camille Chatard, Alain Graillet, Diederik S. Wiersma, and Camilla Parmeggiani\*

Phase behavior modulation of liquid crystalline molecules can be addressed by structural modification at molecular level. Starting from a rigid rod-like core reduction of the symmetry or increase of the steric hindrance by different substituents generally reduces the clearing temperature. Similar approaches can be explored to modulate the properties of liquid crystalline networks (LCNs)—shape-changing materials employed as actuators in many fields. Depending on the application, the polymer properties have to be adjusted in terms of force developed under stimuli, kinetics of actuation, elasticity, and resistance to specific loads. In this work, the crosslinker modification at molecular level is explored towards the optimization of LCN properties as light-responsive artificial muscles. The synthesis and characterization of photopolymerizable crosslinkers, bearing different lateral groups on the aromatic core is reported. Such molecules are able to strongly modulate the material mechanical properties, such as kinetics and maximum tension under light actuation, opening up to interesting materials for biomedical applications.

## 1. Introduction

Liquid Crystal (LC) monomers functionalized by polymerizable groups, such as acrylic or epoxy units, are suitable to prepare a wide range of optical and smart materials.<sup>[1]</sup> Their use allows to develop polymers constituted by molecules aligned with a high degree of order, even in a 3D fashion<sup>[2]</sup> or in a pixelated way.<sup>[3,4]</sup> Indeed, low molecular weight LC monomers can be easily aligned by several techniques<sup>[5,6]</sup> and then polymerized by different approaches (also comprising 3D printing and photolithography) to obtain networks that retain the initial molecular order.<sup>[7]</sup> First reported by Broer et al. in 1988, LC acrylates have been used to prepare different optical filters, retarders and polarizers,<sup>[8,9]</sup> while later on, they have been employed to obtain shape-changing materials. Thanks to

S. Donato, D. Martella, S. Querceto, C. Ferrantini, L. Sacconi, D. S. Wiersma, C. Parmeggiani  
 European Laboratory for Non Linear Spectroscopy (LENS)  
 via N. Carrara 1, Sesto Fiorentino 50019, Italy  
 E-mail: martella@lens.unifi.it; camilla.parmeggiani@unifi.it

S. Donato, D. S. Wiersma  
 Department of Physics and Astronomy  
 University of Florence  
 via G. Sansone 1, Sesto Fiorentino 50019, Italy

D. Martella, D. S. Wiersma  
 Istituto Nazionale di Ricerca Metrologica (INRiM)  
 strada delle cacce 91, Torino 10135, Italy

M. Salzano de Luna  
 Department of Chemical  
 Materials and Industrial Production Engineering  
 University of Naples  
 Piazzale V. Tecchio, 80, Napoli 80125, Italy


G. Arecchi, C. Ferrantini  
 Department of Experimental and Clinical Medicine  
 University of Florence  
 Largo Brambilla 3, Firenze 50134, Italy

L. Sacconi  
 Institute of Clinical Physiology  
 National Research Council (IFC-CNR)  
 V.le Pieraccini 6, Florence 50139, Italy

L. Sacconi  
 Institute for Experimental Cardiovascular Medicine  
 University Heart Center and Medical Faculty  
 University of Freiburg  
 79110 Freiburg, Germany

P.-L. Brient, C. Chatard, A. Graillet  
 Specific Polymers  
 150 Av. des Cocardières, Castries 34160, France

C. Parmeggiani  
 Department of Chemistry “Ugo Schiff”  
 University of Florence  
 via della Lastruccia 3–13, Sesto Fiorentino 50019, Italy

 The ORCID identification number(s) for the author(s) of this article can be found under <https://doi.org/10.1002/marc.202200958>

© 2023 The Authors. Macromolecular Rapid Communications published by Wiley-VCH GmbH. This is an open access article under the terms of the Creative Commons Attribution License, which permits use, distribution and reproduction in any medium, provided the original work is properly cited.

DOI: 10.1002/marc.202200958

the difference in their thermal expansion in parallel and perpendicular direction (with respect to the LC alignment), Liquid Crystalline Network (LCNs) present a shape-change in response to stimuli.<sup>[10,11,12]</sup> Since volume is preserved, a reversible contraction along the nematic director and a consequent expansion in the perpendicular directions are observed under stimulation.<sup>[12]</sup> By engineering the LC alignment, it is therefore possible to obtain 3D deformations under stimuli—such as light when photoresponsive molecules, for example, azobenzenes, are incorporated in the network. After removal of the stimulus, the LC molecules recover the original order and, if the polymeric chains are appropriately crosslinked, the material returns in the initial shape. This kind of materials has been reported for the development of many remotely controlled robotic devices with dimensions from centimeters to micrometers<sup>[13]</sup> and able to accomplish many functionalities, as moving on surfaces by walking, crawling, or jumping,<sup>[14–16]</sup> swimming in liquids,<sup>[17,18]</sup> and even manipulate objects.<sup>[19,20]</sup>

Focusing on the chemistry of LCNs, most reports employ materials prepared by mesogenic diacrylates having a rigid core with three aromatic rings used directly for photopolymerization and crosslinking<sup>[1,9]</sup> or firstly oligomerized by Michael addition (by adding amine or dithiols) and then cross-linked, to obtain main-chain elastomers.<sup>[21,22]</sup> A great challenge remains regarding the LCN optimization in terms of actuation (e.g., contraction or force developed under stimuli), elasticity and strength toward their real application. In this regard, all the molecular parameters have a great importance in determining the LCN performance. Among them, the link of the LC unit to the polymers (from main-chain to side-chain polymers) affects the maximum deformation,<sup>[23,24]</sup> while increasing the spacer length led to an increased order parameter<sup>[25]</sup> and improved deformation at lower temperatures.<sup>[26]</sup> Playing with the crosslinking degree, the material rigidity can be adjusted to allow the 3D printing<sup>[25,27]</sup> or to modulate the extent of deformation.<sup>[27]</sup>

An alternative strategy to improve the LCN properties consists in creating a double interpenetrating network<sup>[28,29]</sup> which however requires extra steps during the fabrication, and that is difficult to be applied for patterned materials or microfabrication. An easier method consists in mixing monomers with different mesogenic cores to decrease the interaction energy in between them thus improving the stimuli responsiveness. Mixing LCs with 2 and 3 aromatic rings in the rigid core was demonstrated as a successful way to decrease the actuation temperature in main-chain LCEs prepared both by acrylate units<sup>[30–32]</sup> or thiol-yne click chemistry.<sup>[33]</sup> In a similar way, the use of a mixture of mesogens based on both aromatic and cyclohexyl rings has been described to decrease the energy needed to obtain the phase transition.<sup>[23]</sup> Recently, for main-chain LCEs, it was also observed that dilution of the mesogenic parts with other co-monomers without LC properties (e.g., ethylene glycol based monomers) allows to decrease the actuation temperatures.<sup>[34,35]</sup>

In this paper, we focus on the optimization of side-chain LCNs prepared by acrylate polymerization, to understand how different mesogenic cores in the crosslinker affect their mechanical properties. The starting point is a formulation already demonstrated able to mimic the force generation of biological muscles<sup>[36]</sup> toward the use of these materials for tissue engineering unsolved needs, as, for example, to support damaged cardiac muscles in

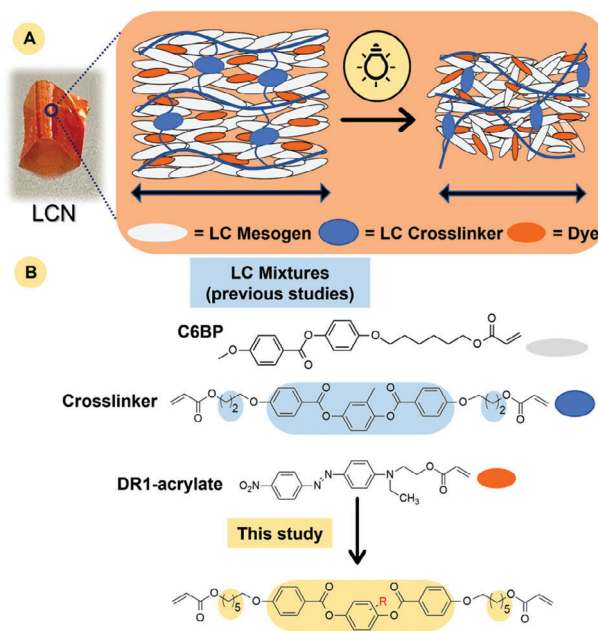


**Figure 1.** Structure of the LCNs. A) A photo-responsive LCN and a scheme of its molecular structure under actuation; B) Structure of the acrylate monomers.

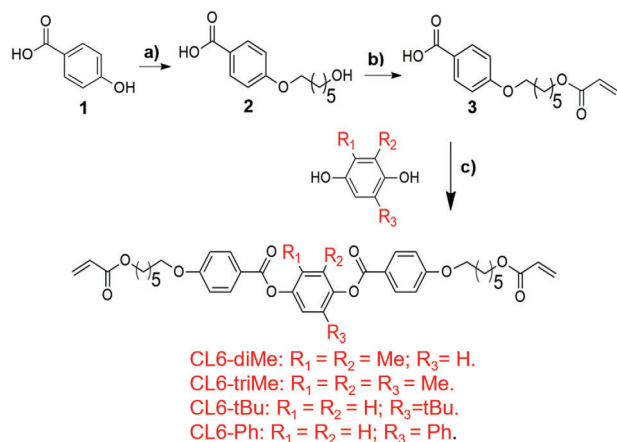
vivo. The challenge of mimicking biological muscles is currently approached by several materials<sup>[37]</sup> but without a really successful solution. If elastomers are most prone to mimic biological tissue elasticity, artificial muscles have also to develop appropriate tension under stimuli and follow a physiologic kinetics of force development. These processes fall in a millisecond time scale that is hard to be reproduced with synthetic artificial muscles.

To improve the LCN performance, we prepared and characterized new LC crosslinkers taking into account the ease of their synthesis and their possible scaling up. Starting from a benzoic acid derivative (presenting an acrylate group), we prepared a small library of crosslinkers by esterification with hydroquinones presenting different bulky substituents. Their insertion in the LCNs has been studied to improve their ability to mimic cardiac tissue force generation and relaxation.

## 2. Results and Discussion

### 2.1. Synthesis and Characterization of Mesogenic Crosslinkers

The LCNs are prepared with a monodomain homogeneous planar alignment which leads to a contraction along the alignment direction during the actuation (Figure 1A). The contraction is related to the mesogen disordering during the stimuli application and can be progressively controlled by the stimulation dose (increasing the temperature or the light intensity allows for higher tension levels).<sup>[23,28]</sup> The materials are synthesized in one step by photopolymerization starting from a mixture of acrylate-based mesogens. A typical composition used in previous studies<sup>[36,38]</sup> and taken here as reference is reported in Figure 1B. It includes a monoacrylate mesogens (C6BP), a diacrylate LC crosslinker (RM257, here called as CL3-Me) and an azobenzene dye (acrylate DR1).



**Scheme 1.** Synthesis of the steric hindered LC-crosslinkers. Reagents and conditions: a) 6-chloro-1-hexanol, KOH, KI, EtOH, H<sub>2</sub>O, reflux, 18 h, 86%; b) acryloyl chloride, NMP, RT, 3 h, 100%; c) DCC, DPTS, CH<sub>2</sub>Cl<sub>2</sub>, hydroquinone derivative, 50 °C, 72 h. Yields: 63% for CL6-diMe, 56% for CL6-triMe, 49% for CL6-tBu, 54% for CL6-Ph.

Starting from this formulation, we investigated the introduction of new LC crosslinkers, prepared by adding on the central aromatic core different numbers and types of substituents.

In this study, crosslinkers are called CLX-Y, where X is the number of carbon atoms in the alkyl chain spacer and Y is the substituents on the central phenyl ring. For example, the reference crosslinker RM257 is called here CL3-Me, where 3 indicate the presence of a propyl spacer in between the core and the acrylate group, and Me indicate one methyl substituent in the central aromatic ring. Accordingly, the monomer mixture and the final materials (that differ only for the crosslinker structure) are called LCNX-Y.

Both CL3-Me and CL6-Me are commercially available molecules (called RM257 and RM82, respectively) and differ only for the spacer length (3 or 6 atoms of carbons in both terminal flexible spacers). The other crosslinkers were synthesized to increase the steric hindrance on the mesogenic core. In particular, we modified the central hydroquinone derived core increasing the number of methyl groups (2 and 3 for CL6-diMe and CL6-triMe, respectively) or changing the substituent on it (a phenyl ring for CL6-Ph or a *tert*-butyl group for CL6-tBu).

Crosslinkers were prepared in 3 steps according to **Scheme 1** and a complete NMR characterization of the compounds is reported in Figure S1–S12, Supporting Information. In all cases, the same building block **3** was esterified with different hydroquinones to get the final products.<sup>[39,40]</sup> Briefly, starting from the 4-hydroxy benzoic acid (**1**), the alkyl spacer was introduced by the Williamson reaction using a chloro-alcohol. The appropriate chemoselectivity was guaranteed by using a combination of water and ethanol as solvent to obtain the substitution on the phenolic group. Molecule **2** was then treated by acryloyl chloride to introduce the polymerizable group leading to the common building block **3**.<sup>[41]</sup> The most critical step was the third one, since the Steglich esterification with sterically hindered hydroquinone should lead to slow reactions and low yields. After the screening of different conditions, the best synthetic approaches were based on the use of the DCC (*N,N*-dicyclohexylcarbodiimide)

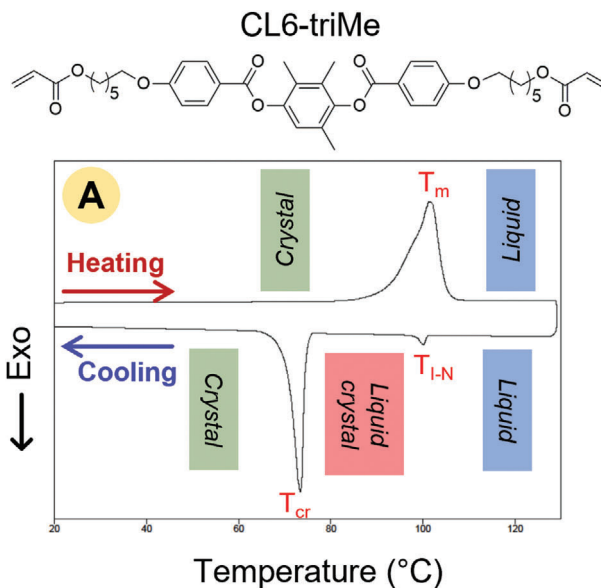


**Figure 2.** Mesomorphic properties of CL6-triMe LC crosslinker. A) DSC trace of the second heating-cooling (20 °C/min) cycle; B) representative POM images of the nematic phase.

or EDC (1-Ethyl-3-(3-dimethylaminopropyl)carbodiimide as the coupling agent, and DPTS (4-(dimethylamino) pyridinium *p*-toluenesulfonate),<sup>[42]</sup> even if only moderate yield were obtained (see Table S1, Supporting Information for a comparison of esterification conditions).

The mesomorphic properties have been studied by Differential Scanning Calorimetry (DSC) and Polarized Optical Microscopy (POM). Combining the results from both techniques, we were able to determine the phase transition temperatures and the type of LC phases as representatively shown in **Figure 2** for the crosslinker CL6-triMe. During the calorimetric analysis (Figure 2A), the molecule presented only one endothermic peak during heating due to the melting in the isotropic phase, while on cooling, two exothermic peaks were present. The first peak indicated an isotropic to liquid phase transition which can be attributed to a nematic phase thanks to the observation of its typical texture by POM (Figure 2B, Schlieren texture with typical 4- and 2-branches defects).<sup>[5]</sup>

The same analysis for the other molecules are reported in Supporting Information (Figures S13–S18, Supporting Information) while the transition temperatures are summarized in **Figure 3** and Table S2, Supporting Information.

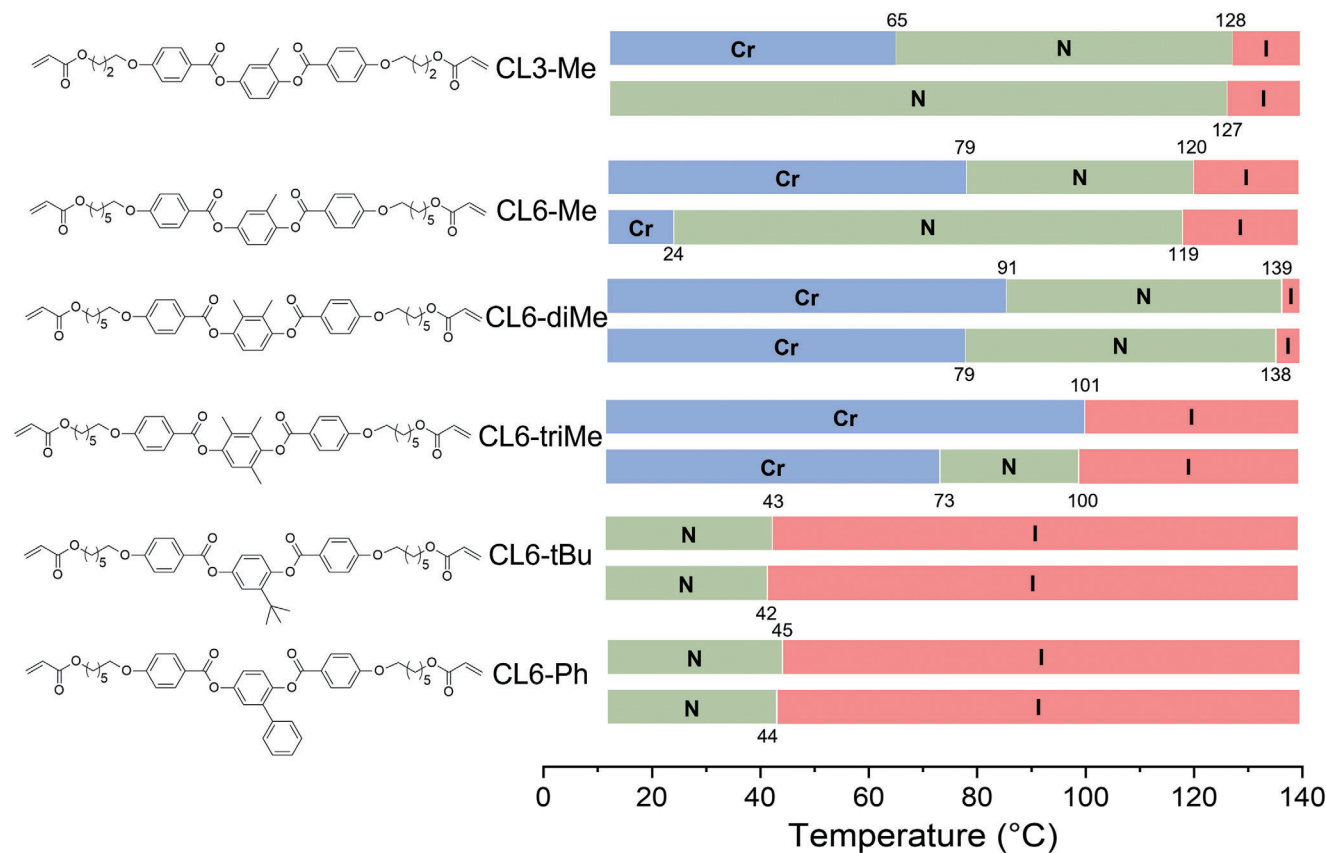


**Figure 3.** Thermal properties of crosslinkers obtained during the second heating (top line)–cooling (bottom line) cycle of DSC experiments ( $20\text{ }^{\circ}\text{C min}^{-1}$ ; Cr: crystalline phase; N: nematic phase; I: isotropic phase). All temperatures are taken at the maximum of the transition peak.

The molecules exhibited enantiotropic behavior, with nematic phase observed both on heating and cooling, with the exception of CL6-triMe, which displays the LC phase only during the cooling step. Within the series of methyl substituted crosslinkers, we observed that melting temperature decreases as the number of methyl substituents increases while clearing temperature does not follow a trend with the substituent number. This behavior was already observed with similar molecules but containing different polymerizable groups.<sup>[35]</sup>

By insertion of the bulkier phenyl and *tert*-butyl substituents, a further clearing temperature reduction is achieved and, very interestingly, both crosslinkers maintain the LC phase even at room temperature for several days. On the contrary, all methyl substituted molecules with 6 carbon atoms exhibit an exothermic crystallization process during cooling. This overall characterization demonstrates our initial hypothesis: the introduction of bulky substituents reduces the clearing temperatures and prevents the crystallization processes. Both requirements allow for an easier material manipulation and fabrication process. Indeed, it is well known how room temperature LCs are preferred for processing by 3D printers or lithographic techniques.<sup>[43,44]</sup>

## 2.2. LCN Fabrication and Mechanical Properties

LCN films were prepared following the steps depicted in Figure 4. Briefly, the monomer mixtures were melted in the

isotropic phase and infiltrated in LC cells assembled by two glasses coated by polyvinyl alcohol (PVA) and rubbed in one direction with a velvet cloth (see Figure S19, Supporting Information for the cell preparation procedure). This way, upon cooling into the nematic phase, we obtained the formation of monodomain homogeneous planar alignment, and by irradiation with UV light, the simultaneous growth of the polymeric chain and their crosslinking were triggered.

We prepared several mixtures having the same ratio (in mol/mol) in between the components but different crosslinker structure. The presence of the Disperse Red 1 (DR1) acrylate allows to control the material deformation by light caused by both the *trans-cis* isomerization of the dye and the photothermal effect.<sup>[7,45]</sup> Once the stimulus is switched off, the material returns in its initial state proving that the process is perfectly reversible for at least 20 days of alternated irradiation.<sup>[36]</sup>

The mixture composition is reported in Table S3, Supporting Information together with the transition temperatures studied by DSC and POM (Figures S20–S24, Supporting Information). All mixtures showed a nematic phase on cooling and no crystallization processes at room temperature.

All the materials were photopolymerized in the same conditions: at  $25\text{ }^{\circ}\text{C}$  for 10 min, followed by a post-curing exposure at  $45\text{ }^{\circ}\text{C}$  to obtain a complete acrylate conversion.<sup>[27]</sup> Some POM images of a monodomain material at the end of the preparation process are shown in Figure S25, Supporting Information,



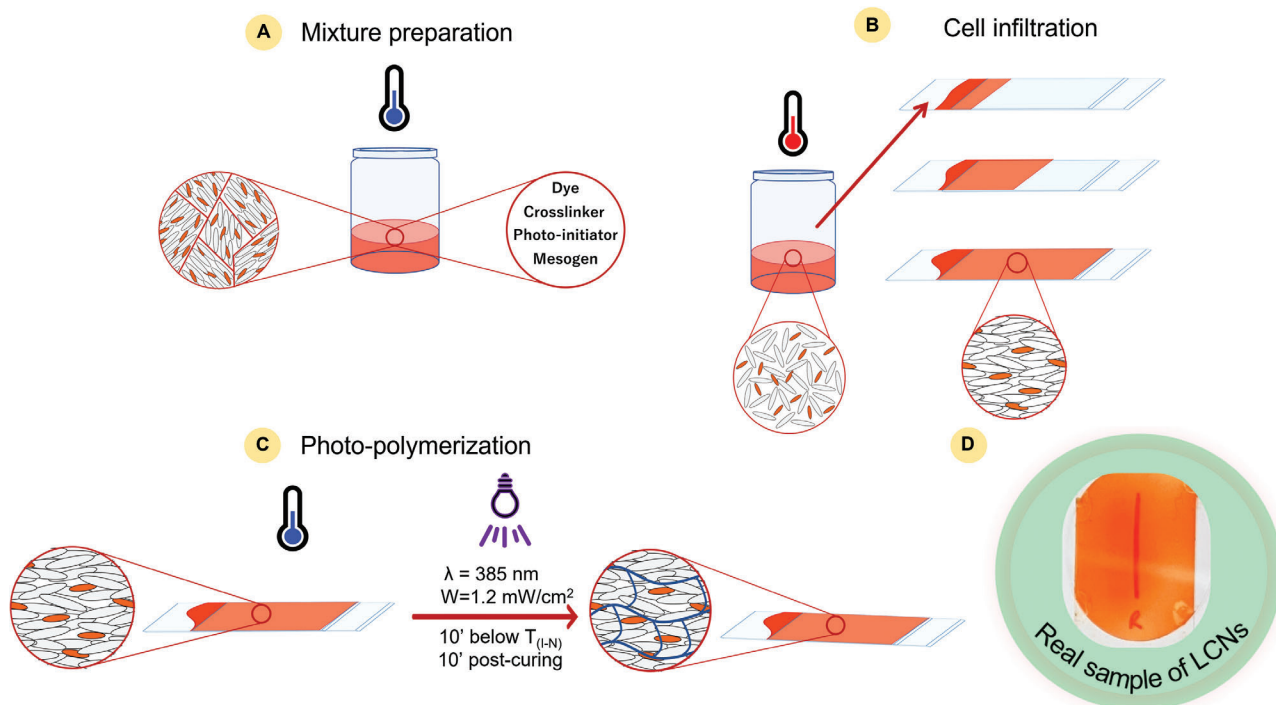


**Figure 4.** LCN preparation steps. A) Mix of monomers dissolved in solvent, and dried under vacuum; B) infiltration of the mixture in a LC cell and formation of the monodomain alignment by cooling down the clearing temperature,  $T_{(I-N)}$ ; C) photopolymerization with the UV lamp; D) real LCN sample picture.

demonstrating the absence of optical defects and a transmittance dependence by the angle in between the polarizers and the nematic directors, as expected for a homogeneous planar alignment. The alignment degree of the materials was monitored by polarized absorption measurement to determine the order parameter ( $S$ ) as reported in Figure S26 and Table S4, Supporting Information. In general, we observed similar  $S$  values, with the exception for the material having tri-methyl substitution that resulted in the less aligned of the series ( $S = 0.34$ ). LCNs with the tert-butyl and the phenyl group in the crosslinker presented a slightly higher alignment degree ( $S = 0.46$ ) than the others.

The glass transition temperatures ( $T_g$ ) measured by DSC analysis for the different films were reported in Figure 5. Starting from our reference material, LCN3-Me ( $T_g = 29^\circ\text{C}$ ), the use of sterically hindered crosslinker led to a moderate decrease of  $T_g$  up to  $10^\circ\text{C}$ . Except for LCN3-Me, all the materials are in their rubbery state at room temperature and no other peaks are present in the DSC traces. This observation suggested that a real nematic to isotropic transition was not present in the materials by increasing the temperature. Generally, for acrylate based LCNs, a gradual decrease of order is obtained by heating up to generate a paranematic state, more disordered than the initial one but never completely isotropic.<sup>[46]</sup>

The increase of the flexible spacer length (from 3 to 6  $-\text{CH}_2-$  groups) led to a moderate  $T_g$  decrease (from 29 to  $20^\circ\text{C}$ ), while no further change was observed by introduction of an additional methyl group (also LCN6-diMe showed a  $T_g$  of  $20^\circ\text{C}$ ). Further increasing the steric hindrance on the central aromatic rings reduced the  $T_g$  with the lowest value observed in case of the phenyl group as the substituent (LCN6-Ph,  $T_g = 10^\circ\text{C}$ ).

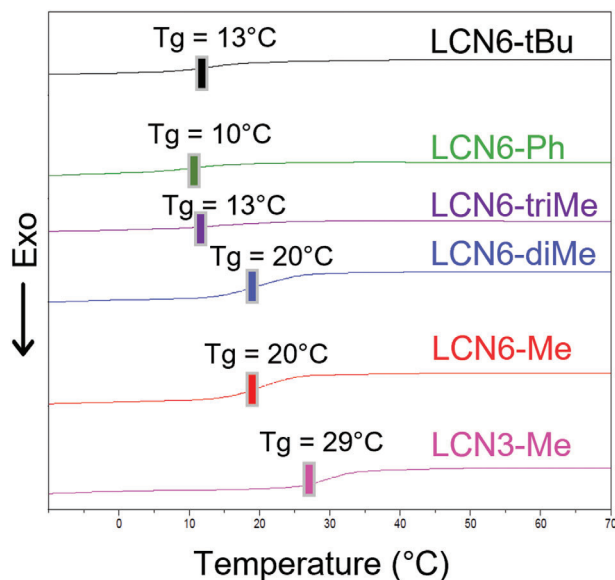


**Figure 5.** DSC traces of LCNs. Heating cycle at  $20^\circ\text{C min}^{-1}$ .

A more detailed mechanical characterization has been performed using a tensiometer for quasi static tensile measurements. For each composition, several tests (at least five replicates) have been performed on films having a thickness of  $10\ \mu\text{m}$  and a width and a length of about 7 and 15 mm, respectively. Each film was analyzed in two directions, either parallel or perpendicular to the nematic director, as reported in Figure 6A. During the tensile

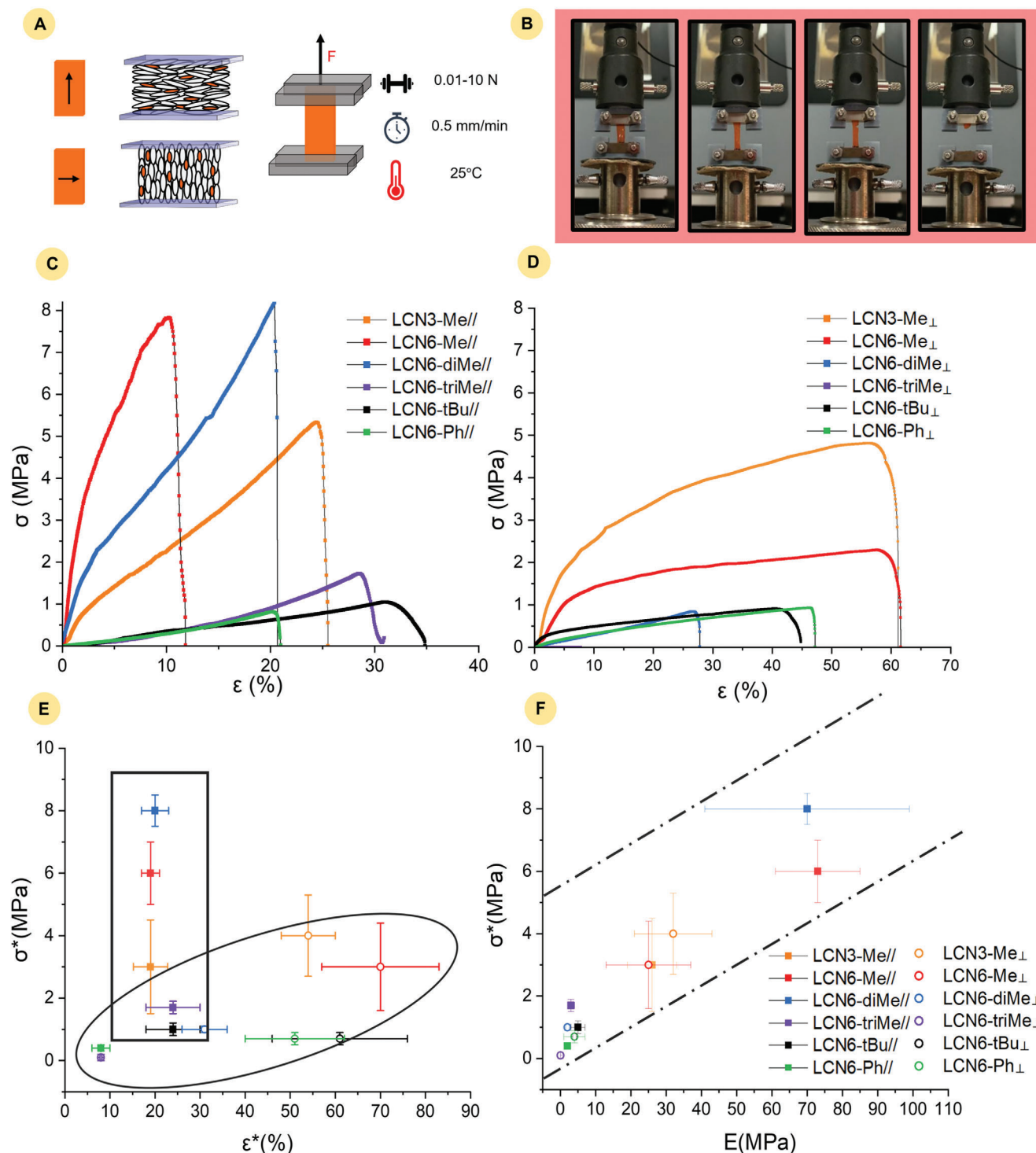


**Figure 6.** Tensile tests on LCNs. A) Summary of the test conditions and B) pictures of a specimen during elongation; C) stress–strain graphs for LCNs analyzed in the direction parallel to the director; D) stress–strain graphs for LCNs analyzed in the direction perpendicular to the director; E) graph reporting the relationship between stress at break ( $\sigma^*$ ) against strain at break ( $\epsilon^*$ ) for all samples; F) graph reporting the relationship between stress at break ( $\sigma^*$ ) and Young modulus ( $E$ ) for all samples.

test (Figure 6B) the material is stretched until breakage, which occurs by formation of a small crack, followed by its expansion until material failure. Representative engineering stress-strain curves are reported in Figures 6C and 6D for films analyzed in the parallel and in the perpendicular direction, respectively. For the sake of clarity, a magnification of the stress-strain curve for LCN6-tBu tested in the perpendicular direction is reported in Figure S27, Supporting Information. From the analyses, different mechanical parameters were retrieved and compared. More specifically, Figure 6E shows the relationship between the stress at break ( $\sigma^*$ ) and the strain at break ( $\epsilon^*$ ), while Figure 6F reports the correlation between stress at break and Young modulus ( $E$ ). The value of all the mechanical parameters are also listed in Table S5, Supporting Information, together with the toughness ( $U$ ) of the materials.

As expected for LC networks and elastomers, the materials present a strongly anisotropic mechanical behavior.<sup>[21,47,48]</sup> When analyzed in the parallel direction, the LCNs exhibit a higher stress at break but a lower strain at break with respect to the same formulation in the perpendicular direction (Figure 6E). Interestingly, the molecular structure of the crosslinker has a major effect on the stress at break of the resulting LCN film when tested in the parallel direction, while the elongation at break is essentially unaffected (reference to the guide for the eye in Figure 6E). With respect to the reference LCN film, indeed, a longer spacer in the crosslinker (LCN3-Me vs LCN6-Me) causes a twofold increase in the average value of  $\sigma^*$ , which further increases up to about 8 MPa when using the crosslinker with two methyl in the rigid core (LCN6-diMe). On the other hand, a higher steric hindrance in the mesogenic core has a detrimental effect on the stiffness of the LCN films (LCN6-triMe, LCN6-tBu, and LCN6-Ph). When focusing on the mechanical properties in the perpendicular direction (reference to the guide for the eye in Figure 6E), instead, it clearly emerges that weakening the interactions among LC cores inside the material (by introducing bulky substituents) determines a significant reduction in the film strength, and in some cases also a lowering of the elongation at break (LCN6-diMe and LCN6-triMe).

Regarding the Young modulus, a general trend can be observed for all the LCNs, for which high values of  $E$  are also accompanied by a high value of stress at break, as evidenced by the track highlighted in Figure 6F. Looking more in detail, as noticed also for the stress at the break, simply increasing the spacer length (LCN3-Me vs LCN6-Me) and slightly acting on the steric hindrance of the substituent (LCN3-Me vs LCN6-diMe) markedly improve the Young modulus in the parallel direction from about 25–70 MPa. However, while for the reference film the value of  $E$  is essentially the same in both directions, the LCN6-Me and LCN6-diMe are significantly less stiff when tested in the perpendicular one. Further increasing the bulkiness of the substituents dramatically softens the films, which exhibited a Young modulus well below 10 MPa irrespective of the testing condition.

### 2.3. Light Actuation

The photomechanical properties of the LCNs were characterized as previously described, by using a customized setup to measure the material force production and the corresponding

kinetics.<sup>[36,38]</sup> In brief, the LCN strips were vertically mounted between a force transducer on top and a fixed end on the bottom (Figure 7A) to measure the force under isometric conditions. The LCN strip was located between two arrays of mini LEDs (mLEDs). Each array was made by eight independent mLED units emitting at  $\lambda = 470$  nm with a pixel pitch of 0.75.<sup>[38]</sup> The LCN films were cut into strips with longer dimensions along the nematic director, that is 8 mm in length  $\times$  1.6 mm in width  $\times$  0.01 mm in thickness. The mLED wavelength was chosen to overlap the maximum absorption region of the dye (Figure 7B).

As already described,<sup>[38]</sup> the force production greatly depends not only on the material composition but also on the illumination conditions, influencing in a not obvious way both the maximum tensions reached and the kinetics of force development. For this reason, light activation has been tested in different illumination conditions. First, the mechanical performances of the LCNs strips were characterized during long-lasting light pulses (that allow the material to reach a nearly-plateau level of force production) under a light power of 14.2 mW mm<sup>-2</sup>. This activation and relaxation pulse of the materials is cyclable and will continue over time without resulting in changes to the force trace obtained, as shown in Figure 7C. This is evidence of the dye resistance to photobleaching, and of its stability.

For each material, a representative trace is reported in Figure 7D while the medium values of maximum force ( $F$ ) and tension ( $T$ ) are provided in Table 1. Upon light illumination, tension initially rises in a nearly linear way, as demonstrated by the analysis of the linear fitting of the curves between 0–100 and 0–200 ms (reported in Figure S28, Supporting Information). In the Supporting Information (Table S6, Supporting Information) a comparison of the kinetic actuation parameters in these ranges is also shown.

First, we observed that maximal tension is reduced in LCN6-diMe and LCN6-triMe strips if compared to the other materials. Furthermore, the rate of activation and relaxation decreases from LCN3-diMe to LCN6-triMe, demonstrating that, as the number of methyl grows, the tension buildup and the response to activation worsens.

On the other hand LCN6-Ph and LCN6-tBu showed maximal tension levels that were similar or even higher than the reference one, and they were chosen for further mechanical characterizations. In this case, the recordings were performed at a much lower light intensity (3.5 mW mm<sup>-2</sup>), moving toward the threshold level for the material activation. This choice was driven by the need to approach intensity levels more suitable for biological applications to develop artificial muscles.

In this condition, the three materials analyzed showed all similar tension levels after 2 s illumination, but the slope of the force trace (measured during the first 200 ms of activation that presents a nearly-linear phase) was significantly higher in LCN6-Ph and LCN6-tBu, underlying a faster kinetics. (Figure 8). Therefore, the LCN6-Ph and the LCN6-tBu, results as the more suitable, among the investigated materials, to be applied in the cardiac tissue engineering field as active contractile layers.

### 3. Conclusion

A palette of LC crosslinkers, was prepared by different substituted hydroquinones and an acrylate containing benzoic acid,

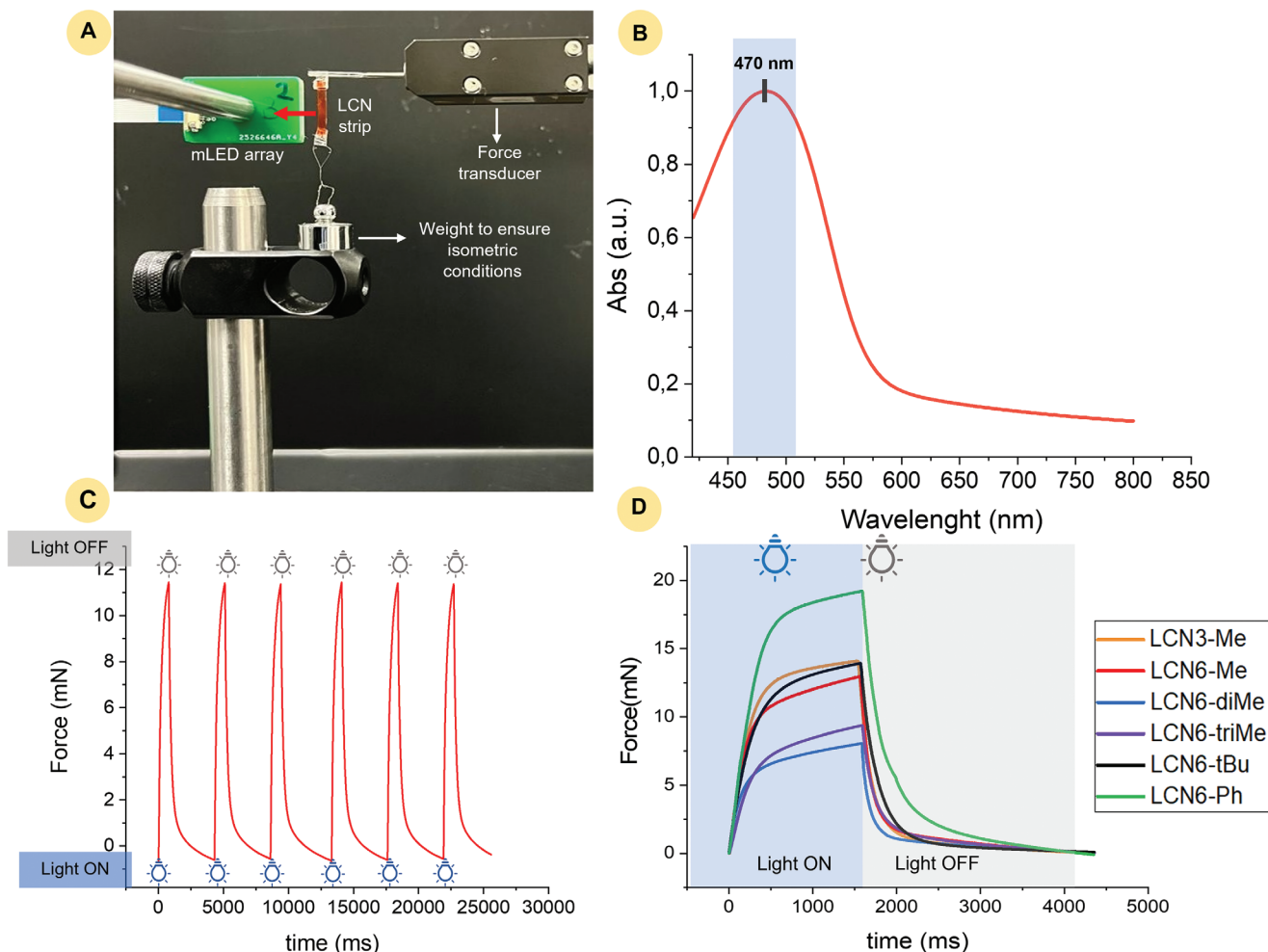


**Figure 7.** Examples of force development under irradiation. A) Images of the setup for force measurement. During the actuation, the sample was positioned in between the two mLED arrays (following the red arrow); B) UV-vis spectra of a LCN6-Ph film; C) trace of multiple activation and relaxation cycles of LCN6-Me under pulsed irradiation by the mLED ( $14.2 \text{ mW mm}^{-2}$ ); D) Force/time graph for materials under blue light. Data reported are referred to representative traces obtained by irradiation of the material with  $14.2 \text{ mW mm}^{-2}$  power and pulsed  $t_{\text{ON}} = 1500 \text{ ms}$  and  $t_{\text{OFF}} = 3000 \text{ ms}$ .

**Table 1.** Force production under light-irradiation. *F*: maximum force developed under the light irradiation ( $14.2 \text{ mW mm}^{-2}$ ) on the plateaus of the trace; *T*: tension development determined dividing the force by the illumination cross-section ( $0.01 \text{ mm thickness} \times 1.6 \text{ mm width}$ ) of the material; values are medium of three samples.

|                | LCN3-Me      | LCN6-Me       | LCN6-diMe    | LCN6-triMe    | LCN6-Ph        | LCN6-tBu      |
|----------------|--------------|---------------|--------------|---------------|----------------|---------------|
| <i>F</i> [mN]  | $14 \pm 1$   | $14 \pm 3$    | $9 \pm 1$    | $10 \pm 2$    | $24 \pm 3$     | $16 \pm 1$    |
| <i>T</i> [KPa] | $896 \pm 68$ | $870 \pm 192$ | $559 \pm 67$ | $643 \pm 150$ | $1480 \pm 220$ | $951 \pm 120$ |

and used to prepare LCNs by photopolymerization. About the mechanical properties, the introduction of bulky substituents in the crosslinker core leads to an increased elasticity, with Young's modulus lower than 4 MPa but with a consequent break at stresses below to 2 MPa. The addition of methyl groups (from 1 to 3) in the crosslinker core, not only lead to a very low stress at break but also to lower force production during illumination, demonstrating as this modification leads to a general worsening of the mechanical ad actuation properties. On the other hand, both LCN6-Ph and LCN6-tBu demonstrated the best photo-actuation

capabilities. These materials still demonstrated a Young's modulus of  $\approx 1 \text{ MPa}$ , significantly higher if compared to cardiac muscles ( $5\text{--}20 \text{ kPa}$ ) but lower if compared to LCN3-Me and faster kinetics with respect to the other materials. This would provide an advantage for applications that require a fast contraction relaxation cycle, like those regarding the mechanical assistance of the cardiac muscle. For instance, if the contraction time course is in the order of  $200\text{--}400 \text{ ms}$  (as in the case of human myocardium), given the slopes that we measured for LCN6-Ph and LCN6-tBu, we expect that both materials would produce 30–40% tension



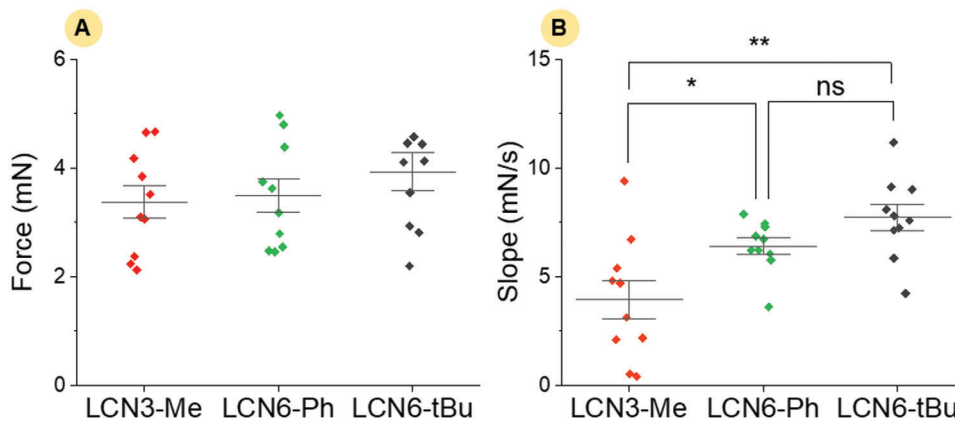


**Figure 8.** Force development at low intensity irradiation. a) Maximum force developed at the plateau and b) slope of the force trace in the first 200 ms of activation for different materials under irradiation at  $3.5 \text{ mW mm}^{-2}$ . Statics analysis: one-way analysis of variance (ANOVA) tests was used to compare features between the three materials ( $N = 10$ ). For the comparison of means between each material the Tukey's post hoc analysis was used. A  $p$ -value of  $< 0.05$  was considered as indicative of a statistically significant difference between means (ns:  $p > 0.05$ ; \* $p < 0.05$ ; \*\* $p < 0.01$ ). Statistical analysis was performed using GraphPad Prism, version 8.4.3.

more than the reference LCN3-Me. Further studies will be concentrated on the modification of the formulation composition to obtain material with higher resistance to mechanical load and more efficient force development under light irradiation.

## 4. Experimental Section

**Materials:** LC components C6BP (4-Methoxybenzoic acid 4-(6-acryloyloxyhexyloxy) phenyl ester), CL3-Me (1,4-Bis-[4-(3-acryloyloxypropyloxy)benzoyloxy]-2-methylbenzene, also known as RM257) and CL6-Me 1,4-Bis-[4-(6-acryloyloxyhexyloxy)benzoyloxy]-2-methylbenzene also known as RM82) were purchased from Synthron Chemicals; Irgacure 369 and all the other reagents were purchased by Merck. Crosslinkers were synthesized as described in Scheme 1 and more details can be found in the Supporting Information (Figures S1–S12, Supporting Information).

**LCN Preparation:** All monomer mixtures contain the mesogen C6BP (88% mol/mol), one of the crosslinker CLX-Y (10% mol/mol), Irgacure 369 (1% mol/mol), and the acrylate dye DR1 (1% mol/mol). To prepare the LC cells, microscope cover slides were coated with an aqueous solution of PVA (5 wt%) and rubbed unidirectionally with a velvet cloth. The cell was assembled by two cover slides separated by  $10 \mu\text{m}$  microspheres as spacers.

The mixture was melted in the isotropic phase and infiltrated by capillary in a LC cell. The material was cooled to room temperature in order to reach a monodomain nematic alignment and photopolymerized for 10 min under UV-light (385 nm, M385LP1-C4 lamp Thorlabs,  $1.2 \text{ mW cm}^{-2}$ ). A post-curing step was applied by UV irradiation for further 10 min at  $45 \text{ }^\circ\text{C}$ .

**Mesomorphic Properties Characterization:** Phase transition temperatures of monomers and LCNs were measured using a DSC TA Instruments Calorimeter Q-2000 (TA Instruments, Milan, Italy) in a nitrogen atmosphere (heating and cooling rate:  $20 \text{ }^\circ\text{C min}^{-1}$ ). POM was performed with an inverted microscope (Zeiss Axio Observer A1) in cross-polarized mode equipped with a Linkam PE120 hot stage and an Axio camera to obtain pictures of the LC textures.

**Mechanical Tensile Test:** A Tensometer 2020 (Alpha Technologies) was used to examine the mechanical behavior of the films during a quasi-static tensile test. The specimen was secured in between two custom-made clamps (Figure 6a,b), and then the mobile upper crosshead started to move at a constant speed of  $0.5 \text{ mm min}^{-1}$ . The force was monitored

throughout the test by a load cell (max force 10 N, 0.02 N accuracy). The engineering stress ( $\sigma = \text{force}/\text{initial specimen section}$ ) and strain ( $\epsilon = \text{displacement}/\text{initial film length}$ ) were calculated from the measured force and displacement data. From the stress-strain data shown in Figure 6c,d, it was possible to determine the stress at break ( $\sigma^*$ ), strain at break ( $\epsilon^*$ ), Young's modulus ( $E$ ), and toughness ( $U$ ) of the various materials. Young's modulus ( $E$ ) was calculated from the stress-strain curves in the initial region where the material demonstrated an analytically linear mechanical response. The modulus was extrapolated using Equation (1), which describes the elastic characteristics of the various LCNs, by using a linear fit of the curve.

$$E = \left. \frac{d\sigma}{d\epsilon} \right|_{\epsilon=\epsilon_i} \quad (1)$$

In addition, the energy required to fracture the material per unit volume, defined as Toughness ( $U$ ) was determined by the area under the stress–strain curve using Equation (2):

$$U = \int_{\epsilon_0}^{\epsilon^*} \sigma d\epsilon \quad (2)$$

**Active Tension Characterization:** The force developed under irradiation by the LCNs were recorded in a custom-made setup previously described.<sup>[36,38]</sup> Briefly, the apparatus consists of a force transducer (WPI KG4, 0–50 mN scale) to which a LCN strip was attached (and held in isometric condition by a weight of  $\approx 5 \text{ g}$ ). Two micro-LED arrays, each composed of eight micro-LEDs emitting blue light (470 nm), were used to irradiate the materials simultaneously on both sides. The activation was controlled by a LabVIEW program with a multichannel driver. Data reported are obtained by irradiation of the material with pulsed light at  $14.2 \text{ mW mm}^{-2}$  (Figure 7) or  $3.5 \text{ mW mm}^{-2}$  (Figure 8).

## Supporting Information

Supporting Information is available from the Wiley Online Library or from the author.

## Acknowledgements

This work has received fundings for the European Union's Horizon 2020 research and innovation programme under grant agreement No. 95216

(REPAIR), from MIUR under the FISIR program, project FISIR 2019\_00320 Leonardo, and from Fondazione Cassa di Risparmio di Firenze projects Ferrantini\_2018.0987 and Parmeggiani\_2020.1583. The authors acknowledge MIUR-Italy ("Progetto Dipartimenti di Eccellenza 2018–2022" for the funds allocated to the Department of Chemistry "Ugo Schiff" and to the Department of Experimental and Clinical Medicine).

Open Access Funding provided by Università degli Studi di Firenze within the CRUI-CARE Agreement.

## Conflict of Interest

The authors declare no conflict of interest.

## Data Availability Statement

The data that support the findings of this study are available from the corresponding author upon reasonable request.

## Keywords

artificial muscles, liquid crystalline crosslinkers, liquid crystalline networks, photoresponsive polymers, structural modifications

Received: February 15, 2023  
Published online: March 25, 2023

- [1] D. Liu, D. J. Broer, *Langmuir* **2014**, *30*, 13499.
- [2] I. Nys, V. Nersisyan, J. Beeckman, K. Neyts, *Soft Matter* **2018**, *14*, 6892.
- [3] B. A. Kowalski, T. C. Guin, A. D. Auguste, N. P. Godman, T. J. White, *ACS Macro Lett.* **2017**, *6*, 436.
- [4] P. Lv, Y. You, J. Li, Y. Zhang, D. J. Broer, J. Chen, G. Zhou, W. Zhao, D. Liu, *Adv. Sci.* **2021**, *8*, 2004749.
- [5] I. Dirking, *Textures of Liquid Crystals*, Wiley, Weinheim **2003**.
- [6] J. Zhao, L. Zhang, J. Hu, *Adv. Intell. Sys.* **2022**, *4*, 2100065.
- [7] T. J. White, D. J. Broer, *Nat. Mater.* **2015**, *14*, 1087.
- [8] D. J. Broer, G. N. Mol, G. Challa, *Makromol. Chem.* **1989**, *190*, 19.
- [9] J. Lub, D. J. Broer, R. T. Wegh, E. Peeters, B. M. I Van Der Zande, *Mol. Cryst. Liquid Cryst.* **2005**, *429*, 77.
- [10] R. S. Kularatne, H. Kim, J. M. Boothby, T. H. Ware, *J. Polym. Sci. B* **2017**, *55*, 395.
- [11] D. Martella, S. Nocentini, C. Parmeggiani, D. S. Wiersma, *Faraday Discuss.* **2020**, *223*, 216.
- [12] G. N. Mol, K. D. Harris, C. W. M. Bastiaansen, D. J. Broer, *Adv. Funct. Mater.* **2015**, *15*, 1155.
- [13] H. Zeng, P. Wasylczyk, D. S. Wiersma, A. Priimagi, *Adv. Mater.* **2018**, *30*, 1703554.
- [14] H. Zeng, P. Wasylczyk, C. Parmeggiani, D. Martella, M. Burrelli, D. S. Wiersma, *Adv. Mater.* **2015**, *27*, 3883.
- [15] J. Jeon, J.-C. Choi, H. Lee, W. Cho, K. Lee, J. G. Kim, J. - W. Lee, K.-I. Joo, M. Cho, H. - R. Kim, J. J. Wie, *Mater. Today* **2021**, *49*, 97.
- [16] K. J. Gwang, J. Jeon, R. Sivakumar, J. Lee, Y. H. Kim, M. Cho, J. H. Youk, J. J. Wie, *Adv. Intell. Syst.* **2022**, *4*, 2100148.
- [17] S. Nocentini, C. Parmeggiani, D. Martella, D. S. Wiersma, *Adv. Opt. Mater.* **2018**, *6*, 1800207.
- [18] S. Palagi, A. G. Mark, S. Y. Reigh, K. Melde, T. Qiu, H. Zeng, C. Parmeggiani, D. Martella, A. Sanchez-Castillo, N. Kapernaum, F. Giesselmann, D. S. Wiersma, E. Lauga, P. Fischer, *Nat. Mater.* **2016**, *15*, 647.
- [19] D. Martella, S. Nocentini, D. Nuzhdin, C. Parmeggiani, D. S. Wiersma, *Adv. Mater.* **2017**, *29*, 28976033.
- [20] O. M. Wani, H. Zeng, A. Priimagi, *Nat. Commun.* **2017**, *8*, 15546.
- [21] T. H. Ware, J. S. Biggins, A. F. Shick, M. Warner, T. J. White, *Nat. Commun.* **2016**, *7*, 10781.
- [22] C. M. Yakacki, M. Saed, D. P. Nair, T. Gong, S. M. Reed, C. N. Bowman, *RSC Adv.* **2015**, *5*, 18997.
- [23] C. Ohm, M. Brehmer, R. Zentel, *Adv. Mater.* **2010**, *22*, 3366.
- [24] D. L. Thomsen, P. Keller, J. Naciri, R. Pink, H. Jeon, D. Shenoy, B. R. Ratna, *Macromolecules* **2001**, *34*, 5868.
- [25] M. Barnes, S. M. Sajadi, S. Parekh, M. M. Rahman, P. M. Ajayan, R. Verduzco, *ACS Appl. Mater. Interfaces* **2020**, *12*, 28692.
- [26] S. Nocentini, D. Martella, C. Parmeggiani, D. Wiersma, *Materials* **2016**, *9*, 525.
- [27] D. Martella, D. Antonioli, S. Nocentini, D. S. Wiersma, G. Galli, M. Laus, C. Parmeggiani, *RSC Adv.* **2017**, *7*, 19940.
- [28] H. - F. Lu, M. Wang, X.u-M. Chen, B. - P. Lin, H. Yang, *J. Am. Chem. Soc.* **2019**, *141*, 14364.
- [29] T. Ube, K. Takado, T. Ikeda, *J. Mater. Chem.* **2015**, *C3*, 8006.
- [30] T. S. Hebner, C. N. Bowman, T. J. White, *Polym. Chem.* **2021**, *12*, 1581.
- [31] G. E. Bauman, J. M. Mccracken, T. J. White, *Angew. Chem., Int. Ed.* **2022**, *61*, 1433.
- [32] F. Lupi, D. Martella, S. Nocentini, D. Antonioli, M. Laus, D. S. Wiersma, C. Parmeggiani, *ACS Appl. Polym. Mater.* **2021**, *3*, 1602.
- [33] R. K. Shaha, A. H. Torbati, C. P. Frick, *J. Appl. Polym. Sci.* **2021**, *138*, 50136.
- [34] M. Barnes, S. Cetinkaya, A. Ajnsztajn, R. Verduzco, *Soft Matter* **2022**, *18*, 5074.
- [35] M. Bispo, D. Guillon, B. Donnio, H. Finkelmann, *Macromolecules* **2008**, *41*, 3098.
- [36] C. Ferrantini, J. M. Pioner, D. Martella, R. Coppini, N. Piroddi, P. Paoli, M. Calamai, F. S. Pavone, D. S. Wiersma, C. Tesi, E. Cerbai, C. Poggiesi, L. Sacconi, C. Parmeggiani, *Circ. Res.* **2019**, *124*, e44.
- [37] J. K. Ponniah, H. Chen, O. Adetiba, R. Verduzco, J. G. Jacot, *J. Mater. Chem. B* **2016**, *4*, 7350.
- [38] G. Vitale, B. Grandinetti, S. Querceto, D. Martella, C. Tesi, C. Poggiesi, E. Cerbai, D. S. Wiersma, C. Parmeggiani, C. Ferrantini, L. Sacconi, *Macromol. Mater. Eng.* **2022**, *307*, 2200187.
- [39] N. Satsangi, H. R. Rawls, B. K. Norling, *J. Biomed. Mater. Res.* **2004**, *71B*, 153.
- [40] J. Kloos, J. Lub, M. Houben, Z. Borneman, K. Nijmeijer, A. P. H. J. Schenning, *Liq. Cryst.* **2022**, <https://doi.org/10.1080/02678292.2022.2134597>.
- [41] Martella, Nocentini, Antonioli, Laus, Wiersma, Parmeggiani, *Polymers* **2019**, *11*, 1644.
- [42] C. J. McAdam, J. Simpson, *Acta Cryst.* **2008**, *64*, 627.
- [43] P. Kiefer, V. Hahn, M. Nardi, L. Yang, E. Blasco, C. Barner-Kowollik, M. Wegener, *Adv. Opt. Mater.* **2020**, *8*, 2000895.
- [44] J. Del Barrio, C. Sánchez-Somolinos, *Adv. Opt. Mater.* **2019**, *7*, 1900598.
- [45] D. Martella, S. Nocentini, F. Micheletti, D. S. Wiersma, C. Parmeggiani, *Soft Matter* **2019**, *15*, 1312.
- [46] I. De Bellis, D. Martella, C. Parmeggiani, E. Pugliese, M. Locatelli, R. Meucci, D. S. Wiersma, S. Nocentini, *J. Phys. Chem.* **2019**, *123*, 26522.
- [47] R. A. M. Hikmet, D. J. Broer, *Polymer* **1991**, *32*, 1627.
- [48] D. Martella, M. Mannelli, R. Squecco, R. Garella, E. Idrizaj, D. Antonioli, M. Laus, D. S. Wiersma, T. Gamberi, P. Paoli, C. Parmeggiani, T. Fiaschi, *iScience* **2021**, *24*, 103077.